ACS Catalysis

Letter

pubs.acs.org/acscatalysis

Co_3O_4 Nanoparticle Water-Oxidation Catalysts Made by Pulsed-Laser Ablation in Liquids

James D. Blakemore, Harry B. Gray, Jay R. Winkler, and Astrid M. Müller*

Beckman Institute, and Division of Chemistry and Chemical Engineering, California Institute of Technology, M/C 139-74, Pasadena, California 91125, United States

Supporting Information

ABSTRACT: Surfactant-free, size- and composition-controlled, unsupported, <5-nm, quantum-confined cobalt oxide nanoparticles with high electrocatalytic oxygen-evolution activity were synthesized by pulsed laser ablation in liquids. These crystalline Co_3O_4 nanoparticles have a turnover frequency per cobalt surface site among the highest ever reported for Co_3O_4 nanoparticle oxygen evolution catalysts in base and overpotentials competitive with the best electrodeposited cobalt oxides, with the advantage that they are suitable for mechanical deposition on photoanode materials and incorporation in integrated solar water-splitting devices.

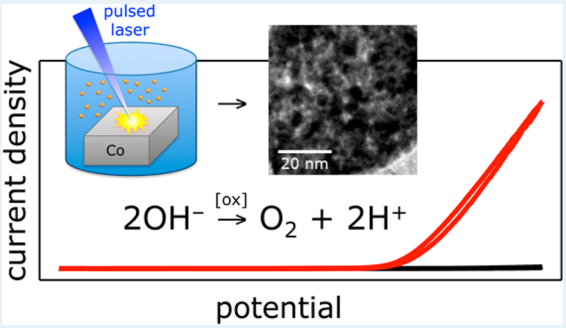

KEYWORDS: *water splitting catalysis, cobalt oxide, electrochemistry, nanoparticles, quantum confinement, oxygen evolution*

Powering the planet in a sustainable way poses a great challenge to humanity in the 21st century.[1] One way that chemistry can meet this challenge is by solar water splitting to generate clean fuels, such as hydrogen. To achieve this goal, protons and electrons[2] to be used in fuel-forming reactions must be liberated from water (or, under alkaline conditions, hydroxide):

$$2OH^- \rightarrow O_2 + 2H^+ + 4e^-$$

Among the materials considered for use as water-oxidation catalysts,[3,4] first-row transition metal oxides can offer high earth abundance and reasonable stability[5] in comparison with their noble-metal analogues.[6] Examples include cobalt oxide-based materials, which continue to attract attention.[7−9] Cobalt oxide can be anodically electrodeposited from cobalt(II) solutions (prepared with nonoxidizable buffers such as phosphate or borate), resulting in high-activity films.[10]

Solution-phase CoO_x nanoparticle syntheses also have been developed; in notable work from Bell and Tilley (BT), ∼10-nm ε-Co, CoO, and Co_3O_4 nanomaterials[11] and 6-nm Co_3O_4 nanoparticles,[12] which were deposited on porous Ni foam electrodes, showed good activity for electrocatalytic water oxidation. Methods for the preparation of cobalt oxide particles on supports,[13] Co(O)OH nanocrystals,[14] and microspheres[15] also have been reported. Many techniques for generating nanostructures use templating or structured substrates.[16]

We report that pulsed-laser ablation in liquids (PLAL) can be used to prepare very small, surfactant-free, size-controlled (<5-nm) Co_3O_4 nanoparticles that show high activity for oxygen evolution from basic water. PLAL is an underexplored technique for nanoparticulate catalyst synthesis with the advantage that nanomaterial suspensions can be prepared with a narrow size distribution without surfactants that could block surface sites and diminish catalytic activity.

In PLAL, focusing an intense laser pulse onto a solid (here: Co metal) that is submerged in a liquid (here: water) creates a plasma plume, which is confined at very high temperatures (∼5000 K) and pressures (∼10 GPa) by the surrounding liquid.[17] Liquid confinement of the plasma plume and absorption of the latter part of the laser pulse generate a shock wave, which leads to rapid cooling and condensation of nanoparticles. Using PLAL, tailored nanomaterials with narrow size distributions can be obtained by tuning and strictly controlling the conditions, including laser pulse length, laser pulse energy, ablation target, and the solution composition.

Earlier work on PLAL in water using Co, CoO, and Co_3O_4 as ablation targets showed that Co, CoO with some Co, and Co particles were produced, respectively, with sizes ranging from nanometers to micrometers;[18] however, size and composition can be controlled by ablating a target Co powder (∼150 μm diameter) that is large compared with the focal beam waist (∼10 μm). It was our view that this arrangement would give the greatest probability of impinging the focused laser pulses on a flat target surface and thus would not interfere with optimal focal properties and subsequent shock wave formation.

Aqueous suspensions of Co_3O_4 nanomaterials were synthesized by focusing 355 nm, 8 ns, 10 Hz repetition rate laser pulses with a 100 mm focal length lens onto 0.5 g of Co powder dispersed by stirring in 10 mL deionized water in ambient air at room temperature. Each sample was irradiated

Received: August 2, 2013
Revised: October 1, 2013
Published: October 3, 2013

   dx.doi.org/10.1021/cs400639b | ACS Catal. 2013, 3, 2497−2500

for 60 min. After synthesis, the remaining Co metal was separated from the newly prepared nanoparticles using a strong magnet (see the Supporting Information (SI) for details).

The resulting materials were then characterized via transmission electron microscopy (TEM) imaging (Figure 1), which showed particles with a diameter of ~2.5 nm after irradiation with a pulse energy of 90 mJ. Not surprisingly, small metal oxide nanoparticles prepared this way aggregate (Figure 1), but as described below, this aggregation does not seem to limit their catalytic activity. Variation of the laser pulse energy leads to Co_3O_4 nanoparticles of different sizes, ranging from (1.4 ± 0.2) to (4.5 ± 0.4) nm with pulse energies varying from 30 to 210 mJ/pulse (SI). For all materials described here, Raman spectra (SI) exhibit peaks consistent with a Co_3O_4 formulation. Further, electron diffraction data show that the particles are randomly oriented crystals (SI).

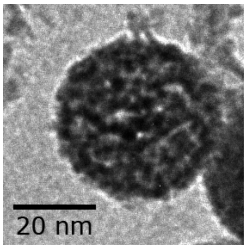

Figure 1. TEM image of Co_3O_4 nanoparticles synthesized by PLAL at 90 mJ/pulse. Note that the very small (2.5 nm) nanoparticles are aggregated because PLAL was performed without addition of surfactants.

Suspensions of the Co_3O_4 nanoparticles are yellow, whereas bulk Co_3O_4 is black. Data suggest this optical spectroscopic property is attributable to quantum confinement (QC). QC has been postulated for other cobalt oxide particles, but we can now provide rigorous experimental evidence.[19] In the optical spectra of our nanoparticles, we find a distinct absorption red shift in the solid state (compared to an aqueous suspension) (SI).[20] Furthermore, we observed an increase in both direct and indirect bandgaps as a function of the reciprocal squared particle diameter. The direct and indirect bandgaps of differently sized Co_3O_4 nanoparticles obtained by Tauc analysis of their absorption spectra were compared with nanoparticle diameters derived from TEM images (SI). We correctly predicted that the critical Co_3O_4 nanoparticle diameter for observation of QC effects would be 5 nm (SI).

We next turned our attention to assaying the electrocatalytic oxygen evolution activity of our particles. Stahl, Dau, and others[21] have demonstrated that neutral or acidic conditions result in corrosion processes and catalyst restructuring that would complicate analysis of particle activity, so we focused on basic conditions. We assessed electrocatalytic activities with respect to mass loading on the relatively flat basal-plane surface of highly ordered pyrolytic graphite (HOPG) electrodes.[22] We chose conditions to minimize the complication of roughness factors when comparing catalyst preparations with different electrode materials.[23]

We drop-cast a solution of freshly prepared nanoparticles (with known concentrations of cobalt from mass spectrometry; see SI) onto an HOPG electrode and collected cyclic voltammetry data for the assembled anode (Figure 2, panel a). A robust catalytic wave onsets below 0.8 V vs NHE that is clearly absent from the bare electrode. Bubbles were visible at the anode after several cycles of voltammetry, suggesting this current flow corresponds to catalytic water oxidation. Importantly, our material is more active than commercial bulk Co_3O_4 (Figure 2, panel b, 10-μm powder) at even higher mass loading, as could be expected for very small nanoparticles with higher microscopic surface areas. Our particles also undergo noncatalytic redox events, in line with observations for related materials.[11,12,21c]

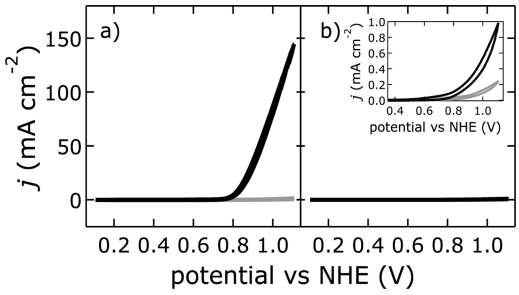

Figure 2. Cyclic voltammograms (second cycle) of (a) 360 ng Co_3O_4 nanoparticles synthesized by PLAL at 90 mJ/pulse (black line) versus bare electrode (gray) and (b) 1000 ng bulk Co_3O_4 (black line) versus bare electrode (gray). Panel b inset shows magnification of data. See the SI for further experimental details. Current densities (j) were obtained by normalization to the geometric electrode area.

Minor changes were observable in the currents over multiple cycles of voltammetry (SI, Figure S6). Because we expected that this finding could indicate structural changes, we turned to TEM to examine particle size as a function of anodic cycle number. Redox-mediated ripening occurred in the first few cycles, which resulted in growth of the as-synthesized particles to a diameter of ~6.5 nm (SI), which were black because they are larger than the critical diameter for quantum confinement.

Knowing the size of the anodized Co_3O_4 particles, we could compare the catalytic activity of our nanoparticulate material with that of commercially available 50-nm Co_3O_4 particles by normalizing current densities to the calculated catalyst surface area (at virtually identical catalyst mass loadings). Our PLAL nanoparticles (SI) exhibited substantially higher activity, presumably as a result of additional exposed edge sites.

We employed a photoluminescence-quench probe to confirm that the current passed in the catalytic wave results in oxygen evolution. We found that the faradaic yield of oxygen based on the total charge transferred was essentially 100% (SI). Moreover, long-term, steady-state measurements confirmed that our assembled anodes were stable beyond 6 h, and during this time, they retained full activity.

Finally, we determined the overpotential and turnover frequency (TOF) of our catalyst. We measured steady-state current as a function of voltage and prepared Tafel plots (Figure 3). The overpotential of our catalyst was 314 mV (measured at 0.5 mA cm^{-2}); for comparison, we electrodeposited a slightly higher loading of cobalt oxide (prepared from a phosphate-buffered solution as described by Nocera and others[10]) and collected Tafel data under our conditions. We found, in line with previous reports, a very similar overpotential of 323 mV. At lower applied voltages, the electrodeposited material showed additional current flow,[21b] resulting in a narrower linear region in the Tafel plot.

TOF values were calculated from steady-state current density and mass-loading data. For Co_3O_4 nanoparticles synthesized by PLAL at 90 mJ/pulse, the mean particle diameter under electrochemical conditions is 6.5 nm, as discussed above.

dx.doi.org/10.1021/cs400639b | ACS Catal. 2013, 3, 2497−2500

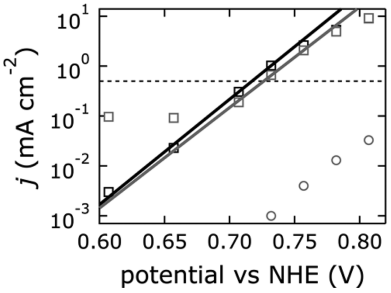

Figure 3. Tafel plots for Co_3O_4 nanoparticles synthesized by PLAL at 90 mJ/pulse (4.5 nmol Co, black), electrodeposited cobalt oxide prepared from a phosphate-buffered solution as described by Nocera and others[10] (4.7 nmol Co, gray squares), and bare HOPG electrode (gray circles). The dashed line indicates a current density of 0.5 mA cm^{-2}. The solid lines are fits to linear regions of the data. Current densities (j) were obtained by normalization to the geometric electrode area.

Assuming a spherical shape and a typical density (Co_3O_4) of 6.11 g cm^{-3}, we calculated the number of Co atoms per particle. Then, using the unit cell length for the Co_3O_4 spinel of 8.084 Å[24] and the number of Co atoms per (100) face, reported by BT,[11] we obtained the number of surface Co atoms per particle, resulting in an estimated TOF of 0.21 mol O_2 (mol $Co_{surface}$)$^{-1}$ s^{-1}.

We surveyed the literature to compare the water oxidation activity of our Co_3O_4 nanoparticles to other Co_3O_4 nanomaterials. For 1 mg of their 10-nm Co_3O_4 particles, BT found (on porous Ni foam anodes with 40 ppcm pore size at pH 14) that catalytic currents reached nearly 350 mA cm^{-2} at 0.9 V vs NHE,[11] whereas we obtained 37 mA cm^{-2} at 0.9 V vs NHE. However, the microscopic surface area of the substrate and catalyst mass loading were greater (loading by a factor of 2800) than for our conditions. On the basis of these numbers, we can directly compare the BT's mass activities with our materials at 0.9 V vs NHE; we obtain 3.50×10^5 mA cm^{-2} g^{-1} for BT's material and 1.02×10^8 mA cm^{-2} g^{-1} for our Co_3O_4 nanoparticles. BT calculated a TOF normalized to the amount of surface-accessible Co of 0.04−0.08 s^{-1} at 300 mV overpotential, compared with our TOF of 0.21 s^{-1} at 314 mV. Our particles likely exhibited a higher TOF, since no surfactants were used that could ligate and block available surface sites. At pH 7, Grzelczak, Wang, and co-workers, who explored 3-nm Co_3O_4 nanoparticles (size was 3 nm following synthesis; no data on ripening were reported), found an overpotential of 660 mV at 1 mA cm^{-2}, which is ∼250 mV higher than observed for Nocera's cobalt oxide material.[8,10]

We conclude that PLAL is a technique with many tunable parameters suited for preparation of very small, surfactant-free, size- and composition-controlled nanomaterials. Our work suggests that these features are especially useful for preparation of nanoparticulate electrocatalysts for solar fuel production. Our <5-nm crystalline Co_3O_4 nanoparticles are highly active catalysts for oxygen evolution in basic water; the particles show high current densities normalized to mass loading, a higher TOF per surface-site Co than previously reported for unsupported Co_3O_4 nanoparticles, and an overpotential similar to that of electrodeposited Co_3O_4. In contrast to findings for the latter material, nanoparticles synthesized by PLAL can be deposited mechanically onto (photo)anodes for assembly of functional devices for solar water splitting.

■ ASSOCIATED CONTENT

Supporting Information

General experimental conditions and apparatus; materials characterization; additional electrochemical characterization; evidence for quantum confinement. This material is available free of charge via the Internet at http://pubs.acs.org.

■ AUTHOR INFORMATION

Corresponding Author

*E-mail: astridm@caltech.edu.

Notes

The authors declare no competing financial interest.

■ ACKNOWLEDGMENTS

We thank Richard P. Gerhart for fabrication of the electrochemical cell used for the oxygen-detection experiment, and Bryce F. Sadtler and Alasdair W. McDowall for help with TEM. Research was carried out in the Laser Resource Center and the Molecular Materials Research Center of the Beckman Institute of the California Institute of Technology. This work was supported by the NSF CCI Solar Fuels Program (CHE-1305124) and the Arnold and Mabel Beckman Foundation.

■ ABBREVIATIONS

PLAL, pulsed-laser ablation in liquids; BT, Bell and Tilley; QC, quantum confinement; TEM, transmission electron microscopy; TOF, turnover frequency; HOPG, highly ordered pyrolytic graphite; NHE, normal hydrogen electrode

■ REFERENCES

(1) (a) Gray, H. B. *Nat. Chem* **2009**, *1*, 7. (b) Lewis, N. S.; Nocera, D. G. *Proc. Natl. Acad. Sci. U.S.A.* **2006**, *103*, 15729−15735.

(2) Schrauben, J. N.; Hayoun, R.; Valdez, C. N.; Braten, M.; Fridley, L.; Mayer, J. M. *Science* **2012**, *336*, 1298−1301.

(3) (a) Trasatti, S. *Electrochim. Acta* **1984**, *29*, 1503−1512. (b) Man, I. C.; Su, H.-Y.; Calle-Vallejo, F.; Hansen, H. A.; Martínez, J. I.; Inoglu, N. G.; Kitchin, J.; Jaramillo, T. F.; Nørskov, J. K.; Rossmeisl, J. *ChemCatChem* **2011**, *3*, 1159−1165. (c) Najafpour, M. M.; Ehrenberg, T.; Wiechen, M.; Kurz, P. *Angew. Chem., Int. Ed.* **2010**, *49*, 2233−2237.

(4) (a) Limburg, J.; Vrettos, J. S.; Liable-Sands, L. M.; Rheingold, A. L.; Crabtree, R. H.; Brudvig, G. W. *Science* **1999**, *283*, 1524−1527. (b) Blakemore, J. D.; Schley, N. D.; Balcells, D.; Hull, J. F.; Olack, G. W.; Incarvito, C. D.; Eisenstein, O.; Brudvig, G. W.; Crabtree, R. H. *J. Am. Chem. Soc.* **2010**, *132*, 16017−16029.

(5) Trotochaud, L.; Ranney, J. K.; Williams, K. N.; Boettcher, S. W. *J. Am. Chem. Soc.* **2012**, *134*, 17253−17261.

(6) Nakagawa, T.; Beasley, C. A.; Murray, R. W. *J. Phys. Chem. C* **2009**, *113*, 12958−12961.

(7) (a) Jiao, F.; Frei, H. *Energy Environ. Sci.* **2010**, *3*, 1018−1027. (b) Pandey, A. D.; Jia, C.; Schmidt, W.; Leoni, M.; Schwickardi, M.; Schüth, F.; Weidenthaler, C. *J. Phys. Chem. C* **2012**, *116*, 19405−19412. (c) Ding, Y.; Xu, L.; Chen, C.; Shen, X.; Suib, S. L. *J. Phys. Chem. C* **2008**, *112*, 8177−8183. (d) Gardner, G. P.; Go, Y. B.; Robinson, D. M.; Smith, P. F.; Hadermann, J.; Abakumov, A.; Greenblatt, M.; Dismukes, G. C. *Angew. Chem., Int. Ed.* **2012**, *51*, 1616−1619.

(8) Grzelczak, M.; Zhang, J.; Pfrommer, J.; Hartmann, J.; Driess, M.; Antonietti, M.; Wang, X. *ACS Catal.* **2013**, *3*, 383−388.

(9) (a) El Wakkad, S. E. S.; Hickling, A. *Trans. Faraday Soc.* **1950**, *46*, 820−824. (b) Shafirovich, V. Y.; Strelets, V. V. *Nouv. J. Chim.* **1978**, *2*, 199−201. (c) Shafirovich, V. Y.; Khannanov, N. K.; Strelets, V. V. *Nouv. J. Chim.* **1980**, *4*, 81−84.

(10) Kanan, M. W.; Nocera, D. G. *Science* **2008**, *321*, 1072−1075.

(11) Chou, N. H.; Ross, P. N.; Bell, A. T.; Tilley, T. D. *ChemSusChem* **2011**, *4*, 1566−1569.

(12) Esswein, A. J.; McMurdo, M. J.; Ross, P. N.; Bell, A. T.; Tilley, T. D. *J. Phys. Chem. C* **2009**, *113*, 15068−15072.
(13) (a) Jiao, F.; Frei, H. *Angew. Chem., Int. Ed.* **2009**, *48*, 1841−1844. (b) Zidki, T.; Zhang, L.; Shafirovich, V.; Lymar, S. V. *J. Am. Chem. Soc.* **2012**, *134*, 14275−14278. (c) Yang, C.-C.; Eggenhuisen, T. M.; Wolters, M.; Agiral, A.; Frei, H.; de Jongh, P. E.; de Jong, K. P.; Mul, G. *ChemCatChem* **2013**, *5*, 550−556.
(14) Alvarado, S. R.; Guo, Y.; Ruberu, T. P. A.; Bakac, A.; Vela, J. *J. Phys. Chem. C* **2012**, *116*, 10382−10389.
(15) Wang, J.; Yang, N.; Tang, H.; Dong, Z.; Jin, Q.; Yang, M.; Kisailus, D.; Zhao, H.; Tang, Z.; Wang, D. *Angew. Chem., Int. Ed.* **2013**, *52*, 6417−6420.
(16) Lee, C.-Y.; Lee, K.; Schmuki, P. *Angew. Chem., Int. Ed.* **2013**, *52*, 2077−2081; **2013**, *52*, 2077−2081 and references cited therein..
(17) Yang, G. W. *Prog. Mater. Sci.* **2007**, *52*, 648−698.
(18) Tsuji, T.; Hamagami, T.; Kawamura, T.; Yamaki, J.; Tsuji, M. *Appl. Surf. Sci.* **2005**, *243*, 214−219.
(19) (a) Patil, V.; Joshi, P.; Chougule, M.; Sen, S. *Soft Nanosci. Lett.* **2012**, *2*, 1−7. (b) Gu, F.; Li, C.; Hu, Y.; Zhang, L. *J. Cryst. Growth* **2007**, *304*, 369−373.
(20) Micic, O. I.; Ahrenkiel, S. P.; Nozik, A. J. *Appl. Phys. Lett.* **2001**, *78*, 4022−4024.
(21) (a) Pourbaix, M. *Atlas of Electrochemical Equilibria in Aqueous Solutions*; Pergamon Press: New York, 1966. (b) Risch, M.; Klingan, K.; Ringleb, F.; Chernev, P.; Zaharieva, I.; Fischer, A.; Dau, H. *ChemSusChem* **2012**, *5*, 542−549. (c) Gerken, J. B.; McAlpin, J. G.; Chen, J. Y. C.; Rigsby, M. L.; Casey, W. H.; Britt, R. D.; Stahl, S. S. *J. Am. Chem. Soc.* **2011**, *133*, 14431−14442. (d) Lutterman, D. A.; Surendranath, Y.; Nocera, D. G. *J. Am. Chem. Soc.* **2009**, *131*, 3838−3839.
(22) McCreery, R. L., in *Electroanalytical Chemistry*; Bard, A. J., Ed.; Dekker: New York, 1991; Vol. *17*; pp 321−373.
(23) Trasatti, S.; Petrii, O. A. *Pure Appl. Chem.* **1991**, *63*, 711−734.
(24) Roth, W. L. *J. Phys. Chem. Solids* **1964**, *25*, 1−10.